

Laminar burning characteristics of ammonia/hydrogen/air mixtures with laser ignition

Wang, Ning; Huang, Shuai; Zhang, Zhifei; Li, Tie; Yi, Ping; Wu, Dawei; Chen, Gen

DOI:

[10.1016/j.ijhydene.2021.07.063](https://doi.org/10.1016/j.ijhydene.2021.07.063)

License:

Creative Commons: Attribution-NonCommercial-NoDerivs (CC BY-NC-ND)

Document Version

Peer reviewed version

Citation for published version (Harvard):

Wang, N, Huang, S, Zhang, Z, Li, T, Yi, P, Wu, D & Chen, G 2021, 'Laminar burning characteristics of ammonia/hydrogen/air mixtures with laser ignition', *International Journal of Hydrogen Energy*, vol. 46, no. 62, pp. 31879-31893. <https://doi.org/10.1016/j.ijhydene.2021.07.063>

[Link to publication on Research at Birmingham portal](#)

General rights

Unless a licence is specified above, all rights (including copyright and moral rights) in this document are retained by the authors and/or the copyright holders. The express permission of the copyright holder must be obtained for any use of this material other than for purposes permitted by law.

- Users may freely distribute the URL that is used to identify this publication.
- Users may download and/or print one copy of the publication from the University of Birmingham research portal for the purpose of private study or non-commercial research.
- User may use extracts from the document in line with the concept of 'fair dealing' under the Copyright, Designs and Patents Act 1988 (?)
- Users may not further distribute the material nor use it for the purposes of commercial gain.

Where a licence is displayed above, please note the terms and conditions of the licence govern your use of this document.

When citing, please reference the published version.

Take down policy

While the University of Birmingham exercises care and attention in making items available there are rare occasions when an item has been uploaded in error or has been deemed to be commercially or otherwise sensitive.

If you believe that this is the case for this document, please contact UBIRA@lists.bham.ac.uk providing details and we will remove access to the work immediately and investigate.

Laminar burning characteristics of ammonia/hydrogen/air mixtures with laser ignition

Ning Wang¹, Shuai Huang^{1,2*}, Zhifei Zhang¹, Tie Li^{1,2*}, Ping Yi^{1,2}, Dawei Wu³, Gen Chen³

1. State Key Laboratory of Ocean Engineering, Shanghai Jiao Tong University

2. Institute of Power Plants and Automation, Shanghai Jiao Tong University

3. Department of Mechanical Engineering, University of Birmingham

*Corresponding Address: 800 Dongchuan Rd., Shanghai, PR China, 200240;

Tel.: (86)21-3420-8348; *E-mail*: zzdett@163.com; litie@sjtu.edu.cn

ABSTRACT

Ammonia, as a zero-carbon fuel, is drawing more and more attention. The major challenge of using ammonia as a fuel for the combustion engines lies in its low chemical reactivity, and therefore more fundamental researches on the combustion characteristics of ammonia are required to explore effective ways to burn ammonia in engines. In this study, the laminar burning characteristics of the premixed ammonia/hydrogen/air mixtures are investigated. In the experiment, the laser ignition was used to achieve stable ignition of the ammonia/air mixtures with an equivalence ratio range from 0.7 to 1.4. The propagating flame was recorded with the high-speed shadowgraphy. Three different processing methods were introduced to calculate the laminar burning velocity with a consideration of the flame structure characteristics induced by the laser ignition. The effects of initial ambient pressure (0.1 MPa-0.5 MPa), equivalence ratio (0.7-1.4), hydrogen fraction (0-20%) on the laminar burning velocity were investigated under the initial ambient temperature of 360K. The state-of-the-art kinetic models were used to calculate the laminar burning velocities in the CHEMKIN-pro software. Both the simulation and experimental results show that the laminar burning velocity of the ammonia mixtures increases at first, reaches the peak around ϕ of 1.1, and then decreases with the equivalence ratio increasing from

24 0.7 to 1.4. The peak laminar burning velocities of the ammonia mixture are lower than 9 cm/s and are
25 remarkably lower than those of hydrocarbon fuels. The laminar burning velocity of the ammonia
26 mixture decreases with the increase of the initial ambient pressure, and it can be drastically speeded
27 up with the addition of hydrogen. While the models except for those by Miller and Bian can give
28 reasonable predictions compared to the experimental results for the equivalence ratio from 0.7 to 1.1
29 in the ammonia (80%)/hydrogen (20%)/air mixtures, all the kinetic models overpredict the
30 experiments for the richer mixtures, indicating further work necessary in this respect.

31 *Keywords:* Ammonia; Hydrogen; Laser ignition; Combustion; Laminar burning velocity

32 **1. Introduction**

33 With the large-scale use of fossil fuels, environmental problems such as the greenhouse effect have
34 become increasingly serious. In 2015, nearly 200 parties to the United Nations Framework Convention
35 on Climate Change agreed to adopt the Paris Agreement, striving to achieve the net zero emissions of
36 greenhouse gases in the second half of this century [1]. The development of new combustion
37 technologies and the utilization of clean energy have become more urgent and important. As clean
38 fuels that do not contain carbon element, ammonia and hydrogen are receiving more and more attention.

39 Ammonia can be used as a hydrogen storage fuel. In the ammonia molecule, the mass content of
40 the hydrogen element reaches 17.7%. Compared with hydrogen, ammonia is of much lower chemical
41 reactivity, and can be liquefied when the pressure reaches 0.857 MPa at 20°C. These properties
42 facilitate a vast potential for the safe and convenient storage as well as transportation [2]. In terms of
43 ammonia production, a complete ammonia production industry has been established worldwide, which
44 are being constantly optimized to reduce carbon emissions in the ammonia production processes [3].

45 In recent years, green ammonia production technologies using clean energy such as solar and wind
46 energy have gradually been promoted and used [4, 5]. Moreover, the specific energy of ammonia is
47 22.5 MJ/kg, which can reach a level comparable to that of some carbon-containing fuels. For example,
48 the specific energy of low-grade coal is about 20 MJ/kg [6]. In terms of the engine applications, the
49 octane number of ammonia is high, and it will not cause severe knocks when working in the spark
50 ignition engines with high compression ratios, thereby a high efficiency can be expected.

51 However, on account of the low chemical reactivity of ammonia, its ignition temperature is high,
52 the flammable range is narrow, the combustion intensity is weak, the flame propagation speed is slow
53 during the combustion processes, and the heat release is slow, which limit its further popularization
54 and application to some extent [7]. In addition, a significant amount of NO_x is inevitably produced
55 during the combustion of ammonia, which is also one of the current challenges. Therefore, more
56 fundamental researches are needed on the combustion of ammonia in order to better understand and
57 utilize it.

58 The chemical reaction mechanism of ammonia combustion has been updated and revised since last
59 century. In the early days, Miller et al. [8] and Bian et al. [9] studied the components in the laminar
60 flame through ammonia combustion experiments. They developed the mechanisms of ammonia
61 oxidation, and clarified the main generation paths of some intermediate products (such as NO, N₂O,
62 etc.). Lindstedt et al. [10] studied the planar laminar premixed flame with different proportions of the
63 ammonia/hydrogen/oxygen mixtures. The mechanism involved 22 chemical components and 95
64 elementary reactions, but it did not simulate the flame structure, which resulted in certain limitations.
65 In recent years, more and more researchers are participating in the study of the ammonia combustion
66 mechanism. Tian et al. [11], Okafor et al. [12], Mei et al. [13], Shrestha et al. [14] and Stagni et al. [15]

67 have updated the kinetic models of ammonia chemical reactions, respectively. Goldmann et al. [16]
68 developed the laminar burning velocity correlations with the ambient pressure, temperature and gas
69 composition for ammonia/hydrogen/air mixtures based on the Mathieu's mechanism [17] and
70 experimental data in literature. However, different kinetic models lead to big differences in
71 predictability of the ammonia combustion characteristics, such as the ignition delay, the laminar
72 burning velocity, the product concentration and so on. Therefore, more systematic experimental data
73 are required to modify these kinetic models under more complete conditions.

74 The laminar burning velocity is crucial to evaluate the combustion for both fundamental research
75 and practical application [18], which can characterize the chemical reactivity of combustibles. Pfahl
76 et al. [19] and Takizawa et al. [20] successively explored the speed of the spherical flame propagating
77 outward when the ammonia/air mixtures were burned at 0.1 MPa. The results confirmed that the
78 laminar burning velocity of ammonia is lower than that of some small molecular hydrocarbon fuels
79 under the same conditions. Hayakawa et al. [21] used a capacitor device to make the spark plug
80 instantly generate sufficient ignition energy to ignite the ammonia/air mixtures. The results showed
81 that the laminar burning velocity decreased as the initial ambient pressure became higher. In addition,
82 the recent study [13, 22-24] showed that an appropriate increase in oxygen concentration, hydrogen
83 fractions or higher initial fuel temperature and can improve the ammonia combustion processes.

84 A wide range of equivalence ratios are usually encountered in practical combustion devices. The
85 diffusion combustion is generally acknowledged to be an effective way in compression ignition
86 engines, turbine engines, boiler combustors and linear free piston engines, where ammonia has great
87 potential to be used. In recent years, the authors in literatures [13, 20, 21, 23-26] have used electric
88 spark to ignite the premixed ammonia/air gas, but the equivalence ratio range they researched was

89 limited from 0.9 to 1.3. Though in the earlier studies, Zakaznov et al. (1978) [27] and Ronney et al.
90 (1988) [28] reported the laminar burning velocities under the richer conditions, they made a very
91 complicated modification to the ignition device that seems not applicable in practice devices.
92 Therefore, it is very difficult to use spark ignition to achieve successful ignition within a wide range
93 of equivalence ratio. There should be a better choice of ignition method and the previous experimental
94 data need to be updated in the modern experimental environment.

95 In this study, the laser ignition is used to broaden the ignitable range of ammonia. The laminar
96 burning characteristics of ammonia are investigated in a wider range of equivalence ratios. Laser
97 ignition is realized by focusing the laser beam with a certain energy into the combustible mixture, and
98 then induce hot plasma. After that, an initial flame kernel forms and the combustion process begins.
99 The electric spark ignition often encounters the electrode ablation and quenching especially at the early
100 stage of the flame development. Compared with the electric spark, the laser ignition, as the “non-
101 intrusive ignition”, would not interfere with the local flow field. It can reduce the heat transfer loss
102 and make the flame propagation more stable during the initial stage [29]. For some combustibles with
103 the low chemical reactivity and weak combustion intensity, such as ammonia, it is easier to achieve
104 stable initial flame by using laser ignition. In addition, laser ignition is also characterized by the
105 flexible and variable ignition position, short ignition delay, precise ignition time control, improved
106 combustion process to reduce emissions, and expanded lean burn limit of the mixture [30]. When it is
107 used in the engine, the auto-ignition and backfire from gas fuelled engine can be overcome. It is also
108 proved that the maximum in-cylinder pressure, the maximum rate of pressure rise and heat release rate
109 are higher with laser ignition, such that the engine performance parameters for laser ignition were
110 superior than spark ignition [31, 32]. However, the existing researches with laser ignition are mostly

111 focused on hydrocarbon fuels, and there are few reports on the ammonia mixtures, while the stable
112 ignition is one of the challenges for ammonia mixtures.

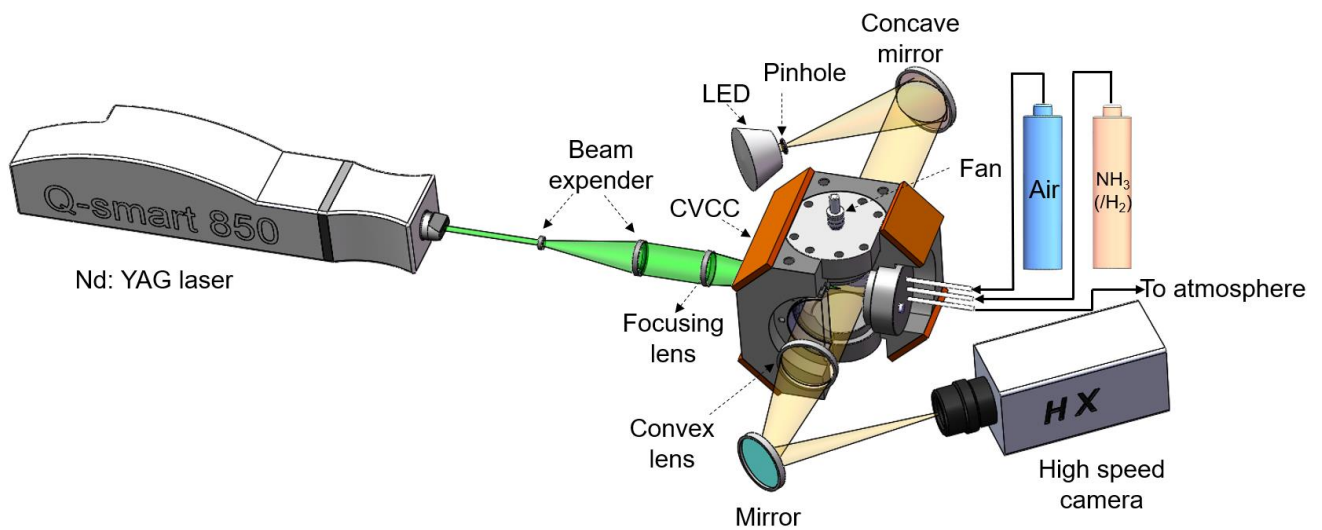
113 The objective of this work is to deepen the study of the laminar flame propagation in the
114 ammonia/hydrogen/air mixtures under a wider equivalence ratios range with laser ignition. This paper
115 investigates the laminar burning characteristics of the premixed ammonia/hydrogen/air mixtures with
116 the experiments and simulations. In the experiment, the laser ignition is used to successfully ignite the
117 ammonia/air mixtures within a wide range of an equivalence ratio range from 0.7 to 1.4. The structure
118 of this paper is as follows. After the Introduction, the experimental apparatus and simulation methods
119 are firstly described, and then three different processing methods considering the flame structure
120 characteristics induced by laser ignition are introduced. In the results and discussion part, the flame
121 morphology changing with time after the laser ignition is analyzed. Then the experimental and
122 simulation results of the laminar burning velocity under different conditions are compared. Moreover,
123 the changes of the flame thickness under different conditions are evaluated. Finally, the main
124 conclusions are summarized.

125 **2. Experimental and numerical methods**

126 *2.1. Experimental methods*

127 **Fig. 1** displays the experimental setup used in this study. The internal volume of the CVCC is 0.9
128 litre, which is approximately a cube with a side length of 97 mm. Three optical windows with a
129 diameter of 90 mm on the CVCC were used to set the laser and shadowgraph light path, and the other
130 side of the CVCC were equipped with the inlet and exhaust pipe, the temperature sensor and pressure
131 sensors. In addition, a mixing fan was installed on the top side of the CVCC to make the mixture as

132 homogeneous as possible and it stopped 30 seconds before the ignition. An electric heater combined
133 with a temperature controller was employed to keep the gas temperature constant at 360 K. The air
134 and ammonia or ammonia/hydrogen mixtures from the high-pressure gas cylinders were respectively
135 charged into the CVCC to create a combustible mixture. The various equivalence ratios of the
136 ammonia/hydrogen/air mixtures can be obtained by controlling the partial pressure of the components.
137 During the intake process, a piezoresistive sensor was used to ensure the accurate measurement of the
138 pressure.



139

140 **Fig. 1.** Schematic of the experimental setup for the laminar flame developments of

141 the ammonia/hydrogen/air mixtures with the laser ignition.

142 In the optical system, the Nd: YAG laser (Quantel Q-smart 850) was employed to generate a pulsed
143 light of wavelength of 532 nm (the second harmonic) and pulse width of 5 ns. The laser beam with a
144 diameter of 6.5 mm was expanded to 50 mm by a beam expander to prevent the excessive laser energy
145 density from damaging the optical window, and then passed through a plano-convex lens with a focal
146 length of 200 mm to focus the laser beam into the CVCC to generate plasma. The focal length of
147 focusing lens is 200 mm and focal diameter of the laser beam is about 1 mm. The laser fluence is about
148 $3.2 \times 10^{13} \text{ W/m}^2$. The flame kernel was formed in the premixed combustible mixture and gradually

149 expanded outward. In the experiment, the energy of the beam before the laser entering the CVCC was
 150 220 mJ in average, which can provide reliable optical breakdown in the range of working conditions
 151 of this study. During the combustion processes, a piezo-electric transducer (KISTLER 6125C) with a
 152 data acquisition instrument was employed to record the dynamic pressure inside the CVCC. According
 153 to the first law of thermodynamics and the ideal gas equation, the heat release rate during the
 154 combustion in the CVCC can be calculated by

$$155 \quad \frac{dQ}{dt} = \frac{1}{\kappa - 1} V_{CVCC} \frac{dp}{dt} \quad (1)$$

156 where Q is the apparent heat released during the combustion; κ is the isentropic index, which is
 157 available on the NIST website [33]; V_{CVCC} is the volume of the CVCC, and p is the real-time ambient
 158 pressure in the CVCC.

159 The shadowgraphs of the laminar flame development processes were recorded by a high-speed
 160 camera (NAC MEMRECAM HX-6). In the experiments, the imaging speed of the camera was set to
 161 5000 fps, and the resolution of the pictures was 832 pixels \times 832 pixels.

162 The experimental conditions are listed in Table 1. The experiment was repeated three times under
 163 each condition and the averaged data were used in the analysis. After each combustion experiment, the
 164 CVCC was evacuated and then filled with air for scavenging.

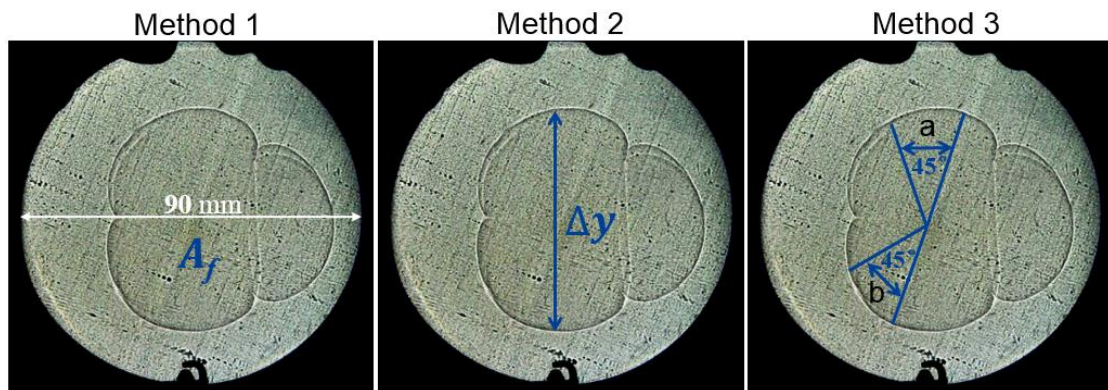
165 **Table 1.** Experimental conditions and imaging parameter settings

Proportion of hydrogen content (%)	0, 10, 20
Equivalence ratio, ϕ (-)	0.7-1.4
Initial ambient pressure, P_0 (MPa)	0.1, 0.3, 0.5
Initial ambient temperature, T_0 (K)	360

166 2.2. Data processing methods

167 In this study, the laminar burning velocity was derived from spherical flame measurements with
 168 the linear extrapolation method to zero curvature. Since the actual flame front is curved, the effect of
 169 flame stretching should be taken into account during the flame propagation. The procedure of the flame
 170 image processing is as follows.

171 First, the image processing is performed to calculate the equivalent radius r_f of the flame. As shown
 172 in Fig. 2, since the flame kernel formed after the laser ignition is usually three-lobe or two-lobe shaped,
 173 three different methods are used in the present study to calculate the equivalent radius.



174

175

Fig. 2. Schematic diagram of the equivalent radius calculation principle.

176 The first is the equivalent area method. The projection area of burned zone (A_f) is firstly calculated
 177 by image processing. Then, the radius of the equivalent circle, r_f , is derived by $r_f = (A_f / \pi)^{0.5}$. To avoid
 178 the ignition impact on the flame development at the initial stage, as well as the buoyancy effect and
 179 the limiting effect by the vessel wall at the later stage, the image with an equivalent radius of 8-20 mm,
 180 termed as quasi-steady state for flame propagation, is processed in this paper [34-36].

181 The second method is to calculate the distance between the top and bottom of the flame kernel as
 182 shown in Fig. 2, and then the equivalent radius, $r_f = \Delta y / 2$.

183 The third method is to use the radius of the curvature of a local place on the front surface of the
 184 flame as the equivalent radius. As shown in Fig. 2, two certain places a and b are selected for
 185 comparative analysis. For better comparison, the ranges of flame kernel development time in the
 186 method 2 and the method 3 are consistent with that of the method 1.

187 Once the equivalent radius is obtained, the stretched flame speed (S_b) can be calculated by the
 188 change rate of the equivalent radius with time:

$$189 \quad S_b = \frac{dr_f}{dt} \quad (2)$$

190 The stretch rate of the flame (ε) characterizes the change rate of the projection area of the burned
 191 zone:

$$192 \quad \varepsilon = \frac{1}{A_f} \cdot \frac{dA_f}{dt} = \frac{2}{r_f} \cdot \frac{dr_f}{dt} \quad (3)$$

193 The relationship between the unstretched flame speed (S_b^0) and the stretched flame speed (S_b) can
 194 be expressed by

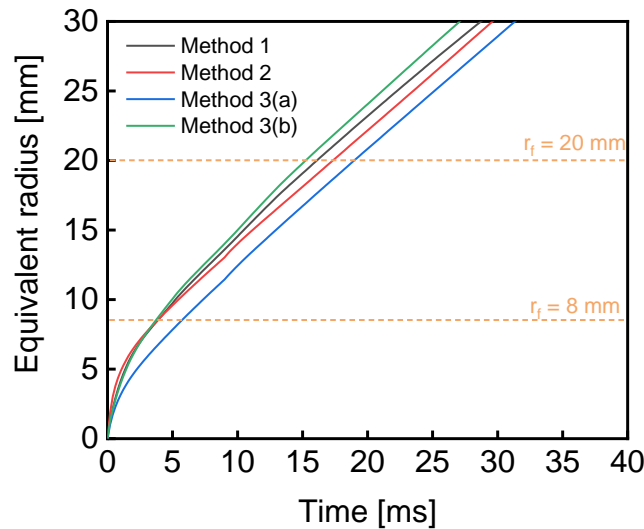
$$195 \quad S_b^0 - S_b = L_b \cdot \varepsilon \quad (4)$$

196 The proportional constant L_b in the above formula is the Markstein length. Therefore, S_b^0 can be
 197 obtained by the linear extrapolation using the progressive analysis [37, 38]. When ε approaches 0, S_b
 198 is nearly equal to S_b^0 .

199 Finally, the laminar burning velocity can be calculated by multiplying the unstretched flame speed
 200 with the ratio of the burned gas density to the unburned gas density:

$$201 \quad S_L = S_b^0 \cdot \frac{\rho_b}{\rho_u} \quad (5)$$

202 The uncertainty in the stretch extrapolation can be coupled with the uncertainties caused by ignition,
 203 radiation, and confinement effects [39]. The flame is in an unstable state at the early stage, and the
 204 stretched speed subjects to great effects caused by the ignition. Bradley et al. [34, 35] suggested that
 205 the ignition effects can be avoided when the flame radius are larger than 6 mm. Accordingly, the
 206 selected smallest radius here is 8 mm. In addition, to reduce the effect of wall confinement, the largest
 207 flame radius is limited at 20 mm [36]. Fig. 3 shows the temporal evolution of the equivalent radius
 208 change for three methods. Flame propagation is in a quasi-steady state with an equivalent radius of 8-
 209 20 mm.



210
 211 **Fig. 3.** Development of the equivalent radius of three methods for the combustion of the ammonia/air
 212 mixtures ($\phi = 1.0$, $P_0 = 0.1$ MPa, $T_0 = 360$ K).

213 2.3. Numerical simulation methods

214 In this study, a freely propagating adiabatic, premixed, planar flame of the ammonia/hydrogen/air
 215 mixtures was simulated using the one-dimensional freely propagating laminar flame model in the
 216 CHEMKIN-pro software. Six different chemical reaction mechanisms were adopted in the simulation,
 217 including the ammonia chemical reaction kinetic models published by Miller et al. [8], Bian et al. [9],

218 Okafor et al. [12], Mei et al. [13], Shrestha et al. [14] and the GRI 3.0 mechanism [40]. The
 219 corresponding Gas-Phase Kinetic File, Thermodynamics Data File and Gas Transport Data File of the
 220 above six kinetic models were used in the simulations.

221 The operating conditions of the simulations were set the same as those of the experiments, as shown
 222 in Table 2. Table 2 also lists some relevant physical characteristics of the ammonia/hydrogen/air
 223 mixtures under each operating condition. λ , C_p , α and ν are the thermal conductivity, specific heat at
 224 constant pressure, thermal diffusivity, and kinematic viscosity, respectively. ρ_u and ρ_b are the density
 225 of unburned gas and the density of burned gas, respectively. For single species, the Lewis number can
 226 be calculated by

$$227 \quad Le_i = \frac{\lambda}{\rho_u C_p D_m} \quad (6)$$

228 where D_m is the diffusion coefficient of insufficient reaction material (lean or rich mixture). For a
 229 mixture of a single component fuel and an oxidizer, Le is defined based on the deficient reactant as
 230 the ratio of the thermal diffusivity of the mixture to the molecular diffusivity of the deficient reactant
 231 in the mixture. According to Bechtold et al. [41], Le is given by

$$232 \quad Le = 1 + \frac{(Le_E - 1) + (Le_D - 1)A}{1 + A} \quad (7)$$

233 where $A = 1 + Ze (\phi - 1)$. The Lewis numbers Le_E and Le_D are those defined based on the excess
 234 reactant and the deficient reactant, respectively.

235 Ze is the Zel'dovich number which is obtained from

$$236 \quad Ze = 4 \frac{T_{ad} - T_u}{T_{ad} - T_{inner}} \quad (8)$$

237 where T_{ad} and T_{inner} are the adiabatic flame temperature and the inner layer temperature, respectively.

238 The geometrical definition of the inner layer temperature was employed in obtaining the values

239 of T_{inner} for each mixture. Goey et al. [42] suggested that values of T_{inner} can be obtained based on the
 240 geometrical definition.

241 For two-component fuels, this paper adopts the effective Lewis number (Le_{eff}) of multi-
 242 component fuels based on the volume weighting calculation [43]:

$$243 \frac{1}{Le_{eff}} = \frac{X_{NH_3}}{Le_{NH_3}} + \frac{X_{H_2}}{Le_{H_2}} \quad (9)$$

245 where X_{NH_3} and X_{H_2} are the volume fractions of ammonia and hydrogen in the mixed fuel, and Le_{NH_3} and
 246 Le_{H_2} are the Lewis numbers corresponding to ammonia and hydrogen, respectively.

247 The thermal expansion rate, σ , characterizes the ratio of burned gas density to the unburned gas
 248 density, which indicates the density fluctuation on both sides of the flame front:

$$249 \sigma = \frac{\rho_b}{\rho_u} \quad (10)$$

250 In addition, δ is the thermal diffusion flame thickness [44], which can be calculated by

$$251 \delta = \frac{\lambda}{\rho_u C_p S_L} = \frac{\alpha}{S_L} \quad (11)$$

252 In Table 2, the initial ambient pressure, initial ambient temperature and equivalence ratio are the
 253 input parameters for the simulations. ρ_u , ρ_b , λ , C_p , α and ν can be calculated by CHEMKIN-pro. The
 254 mechanism by Mei et al. [13] was used here. Le and δ can be obtained by further calculations with the
 255 above simulation results.

256 **Table 2.** Physical characteristics of the ammonia/hydrogen/air mixtures

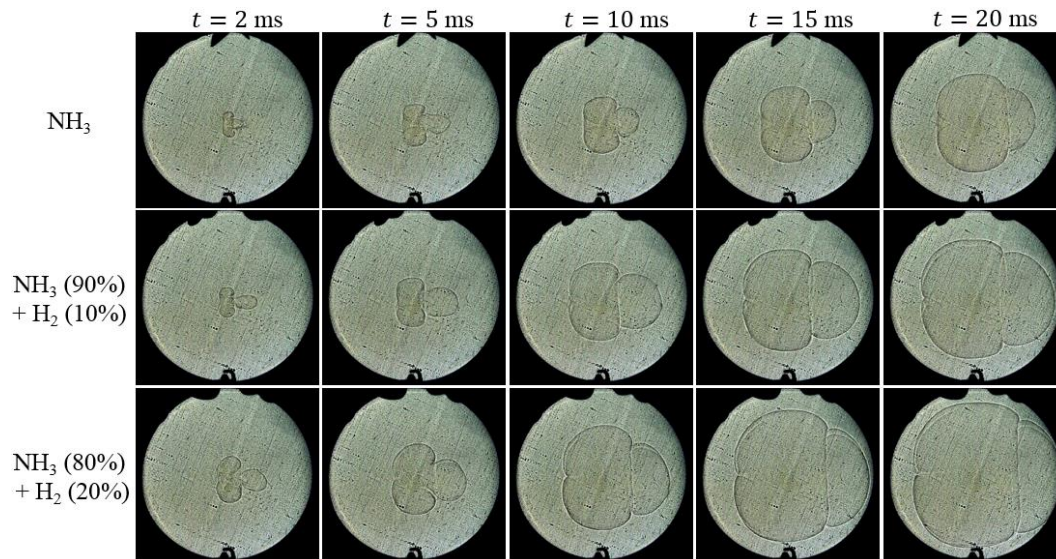
X_{H_2} (%)	P_0 (MPa)	ϕ (-)	ρ_u (kg/m ³)	ρ_b (kg/m ³)	λ (10 ⁻² W/m/K)	C_p (W/kg/K)	ν (10 ⁻⁵ m ² /s)	α (10 ⁻⁵ m ² /s)	Le_{eff}	σ (-)	δ (10 ⁻⁴ m)
0	0.1	0.7	0.911	0.178	3.16	1140	2.19	3.04	0.861	5.12	8.86
	0.1	0.8	0.903	0.164	3.18	1156	2.19	3.04	0.927	5.51	5.63
	0.1	0.9	0.896	0.153	3.19	1171	2.19	3.04	0.959	5.86	4.15

	0.1	1	0.889	0.145	3.20	1186	2.19	3.04	0.978	6.13	3.26
	0.1	1.1	0.882	0.144	3.22	1200	2.19	3.04	0.991	6.13	2.68
	0.1	1.2	0.876	0.145	3.23	1214	2.19	3.03	0.999	6.04	2.71
	0.1	1.3	0.87	0.147	3.24	1228	2.19	3.03	1.005	5.92	2.99
	0.1	1.4	0.864	0.149	3.25	1241	2.19	3.03	1.009	5.80	3.41
	0.3	1	2.667	0.432	3.20	1186	0.73	1.01	0.978	6.17	1.40
	0.5	1	4.45	0.718	3.20	1186	0.44	0.61	0.978	6.20	0.94
10	0.1	1	0.875	0.144	3.43	1199	2.24	3.26	0.713	6.08	2.66
	0.3	1	2.63	0.428	3.43	1199	0.74	1.09	0.713	6.14	1.18
	0.5	1	4.38	0.712	3.43	1199	0.45	0.65	0.713	6.15	0.80
20	0.1	0.5	0.913	0.216	3.37	1120	2.24	3.30	0.213	4.23	15.71
	0.1	0.6	0.9	0.192	3.45	1141	2.25	3.36	0.232	4.69	7.39
	0.1	0.7	0.89	0.175	3.51	1160	2.26	3.40	0.275	5.09	4.48
	0.1	0.8	0.88	0.161	3.56	1178	2.27	3.43	0.312	5.47	3.19
	0.1	0.9	0.87	0.15	3.61	1196	2.28	3.47	0.399	5.80	2.51
	0.1	1	0.861	0.142	3.66	1213	2.28	3.51	0.447	6.06	2.08
	0.1	1.1	0.852	0.141	3.71	1230	2.29	3.54	0.478	6.04	1.86
	0.1	1.2	0.844	0.14	3.76	1247	2.30	3.57	0.500	6.03	1.89
	0.1	1.3	0.836	0.141	3.80	1263	2.31	3.60	0.517	5.92	2.04
	0.1	1.4	0.828	0.143	3.84	1279	2.32	3.63	0.530	5.79	2.27
	0.1	1.5	0.821	0.144	3.89	1294	2.32	3.65	0.541	5.70	2.57
	0.3	1	2.58	0.423	3.66	1213	0.76	1.17	0.447	6.10	0.97
	0.5	1	4.3	0.705	3.66	1213	0.46	0.70	0.447	6.10	0.66

257 3. Results and discussion

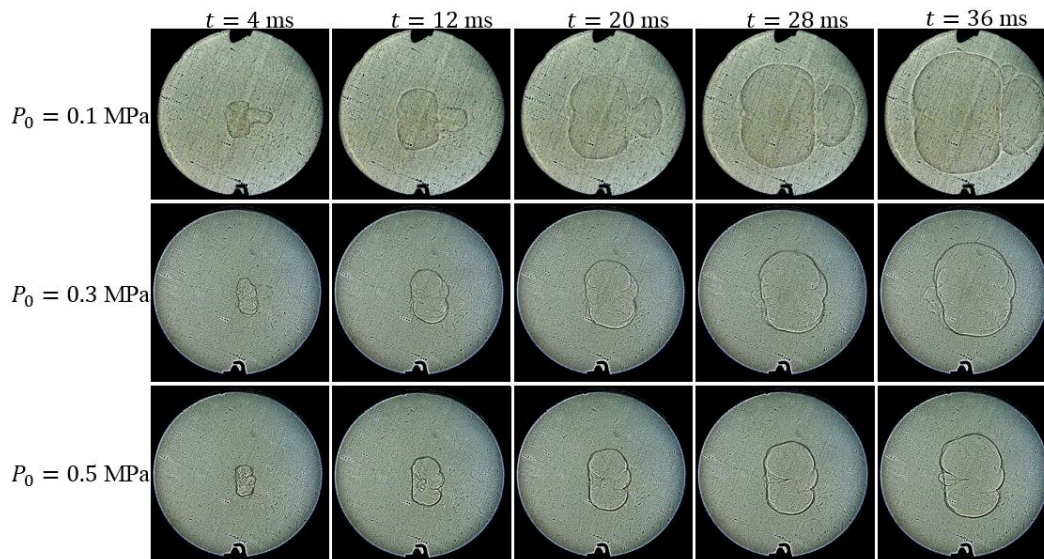
258 3.1. Flame morphology

259 Fig. 4(a) shows the flame evolutions for the three fuels with different hydrogen fractions under P_0
260 of 0.1 MPa. The flame kernel has a three-lobe shape and gradually spreads outward. At a fixed moment,
261 the higher the hydrogen proportion, the farther the flame spreads. Among them, the fuel with a
262 hydrogen content of 20% spreads fastest. The flame front is close to the vessel wall at 20 ms. Fig. 4
263 (b) shows the development of the flame in the ammonia/air mixtures under different initial ambient
264 pressures. With the initial ambient pressure increasing, the flame propagation is slower.



265
266 **Fig. 4 (a).** Temporal development of the flame for the three fuels

267 ($\phi = 1.0, P_0 = 0.1 \text{ MPa}, T_0 = 360 \text{ K}$).



268
269 **Fig. 4 (b).** Temporal development of the flame in the ammonia/air mixtures under different initial

270 ambient pressures ($\phi = 1.0, T_0 = 360 \text{ K}$).

271 **Fig. 5 (a) & (b)** shows the development of the projection area of the burned zone and the equivalent

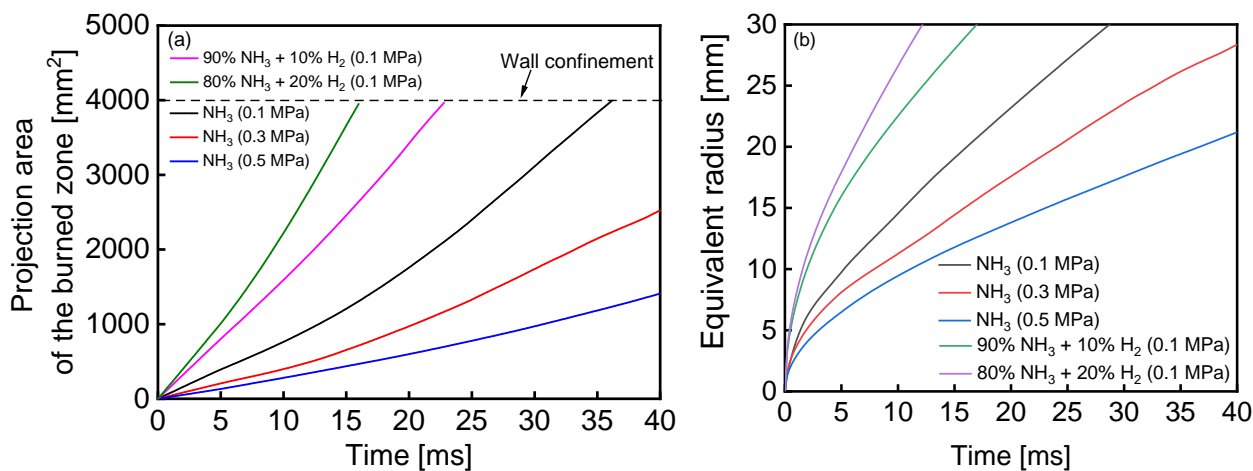
272 radius under different experimental conditions, respectively. It can be seen that the projection area of

273 the burned zone and the equivalent radius is positively correlated with the hydrogen proportions, and

274 negatively correlated with the initial ambient pressures at a fixed moment. When the proportion of

275 hydrogen contents is higher and the initial ambient pressure is lower, the flame kernel spreads faster.

276 When the projection area of the burned zone increases to 4000 mm², the flame front surface approaches
 277 the wall of the CVCC.



278
 279 **Fig. 5.** Development of the projection area of the burned zone (a) and equivalent radius (b) for the
 280 combustion of the ammonia/hydrogen/air mixtures under different initial ambient pressures ($\phi = 1.0$,
 281 $T_0 = 360$ K).

282 As shown in Fig. 6, the cellular instability of laminar flame was observed in this study. Two kinds
 283 of instabilities are probably involved here: 1) the diffusion-thermal instability and 2) the hydraulic
 284 instability [44, 45]. The diffusion-thermal instability can be evaluated by the Lewis number [46]. When
 285 Le is less than a certain critical value (slightly less than 1), the thermal diffusion at the front of the
 286 flame is weaker than the mass diffusion, and the flame propagation is prone to instability. The hydraulic
 287 instability is caused by the inconsistent density on both sides of the flame front [45]. When the density
 288 of the unburned area and the burned area fluctuate greatly and the thickness of the flame is thinner, the
 289 front of the flame is easily disturbed and wrinkles appear [47]. At the initial stage of the flame
 290 development, due to the small radius of the flame kernel and the large stretching rate, the flame front
 291 surface is affected by the strong curvature limitation and stretched effect, and it tends to stability [44],
 292 while the diffusion-heat instability and hydraulic instability are limited [48].

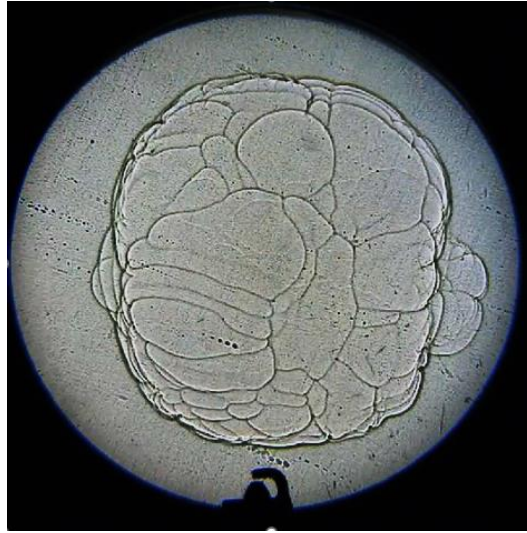


Fig. 6. Cellular instability of the laminar flame in this study

($X_{H_2} = 20\%$, $P_0 = 0.1$ MPa, $\phi = 1.0$, $t = 35$ ms).

In this study, the simulation results of the Lewis number Le and flame thickness δ are given in [Table 2](#). When the equivalence ratio is 1.0, for the same fuel, the corresponding Le is the same under different pressures, indicating that the effect of diffusion-thermal instability is the same. The thermal expansion rate characterizes the ratio of the density of unburned gas to the density of burned gas. With the initial ambient pressure increasing, the thermal expansion rate does not change much, while the flame thickness will decrease, making it more susceptible to hydraulic instability. In addition, for three different fuels, the flame thickness decreases as the hydrogen proportion increases with the same initial ambient pressure and equivalence ratio, making it more prone to instability.

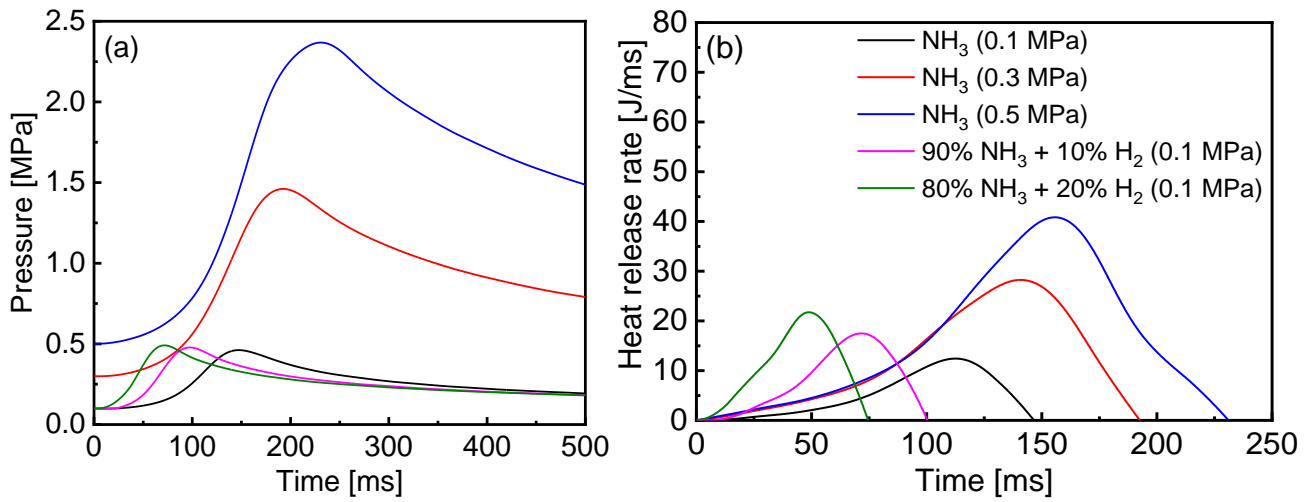
In this study, the instability was observed at the later stage of flame development when the initial ambient pressure was 0.5 MPa and the proportion of hydrogen contents was 20% as shown in [Fig. 7](#). Since this kind of cellular instability occurred at the later stage of flame development, the equivalent radius of the flame kernel was large at that time. In the range of the equivalent radius from 8 to 20 mm,

308 the flame instability is limited, and the above methods can be used to calculate the laminar burning
309 velocity.

310 3.2. Pressure trace and heat release rate

311 [Fig. 7](#) show the pressure traces and heat release rates during the combustion of the
312 ammonia/hydrogen/air mixtures, respectively. After the mixture is ignited, the flame spreads outward.
313 The fuel burns and begins to release heat, and the pressure in the CVCC gradually rises. When the
314 pressure reaches the peak, the heat releasing process ends. The peak pressure increases as the initial
315 ambient pressure increases for the ammonia/air mixtures as shown in [Fig. 7\(a\)](#). For the fuels with
316 different proportions of hydrogen contents, the higher the hydrogen fraction, the higher the pressure
317 peaks during the combustion process, and the shorter the time it takes to rise to the peak. This can be
318 attributed to the stronger combustion intensity of hydrogen. It is worth noting that at 0-20 ms after the
319 ignition, the pressure in the CVCC increases below 5% of the peak pressure. Therefore, the pressure
320 during this period can be approximated as constant. This time period is also the stage of data processing
321 in this paper.

322 As shown in [Fig. 7\(b\)](#), the duration of heat releasing increases with the initial ambient pressure
323 increasing. This is caused by the increase in the total amount of reactants and the slow flame
324 propagation speed under the higher initial pressure. In addition, owing to the higher chemical reactivity
325 of hydrogen, when the hydrogen fraction is higher, the heat releasing process is faster. According to
326 the NIST website [\[33\]](#), here the value of the isentropic index (κ), is 1.271, 1.284 or 1.296 in Eq. (1)
327 when the proportion of hydrogen contents in the fuel blends is 0, 10% or 20%, respectively. When the
328 temperature changes in the range of 360 K to 2000 K, the change of the isentropic index is below 7%.



329

330

Fig. 7. Pressure change (a) and Heat release rate change (b) in CVCC during the combustion of the

331

ammonia/hydrogen/air mixtures under different initial ambient pressures ($\phi = 1.0$, $T_0 = 360$ K).

332

3.3. Laminar burning velocity

333

3.3.1 Effects of equivalence ratio

334

Fig. 8(a) shows the laminar burning velocities of the ammonia/air mixtures with various

335

equivalence ratios. Plotted are four kinds of results obtained by the proposed methods based on the

336

experimental data of this research. The initial ambient pressure is 0.1 MPa and the initial ambient

337

temperature is 360 K. There are some variations in the laminar burning velocity at the fixed

338

equivalence ratio for the three data processing methods. These variations by different processing

339

methods in this study are well in the range of the variation of the laminar burning velocity at fixed

340

equivalence ratio in the literatures [13, 21, 23, 25, 28] where the electric spark was used to generate a

341

spherical flame to evaluate the laminar burning characteristics. The entire flame front was considered

342

in method 1, which averaged the results of all locations, while method 2 and method 3 were just based

343

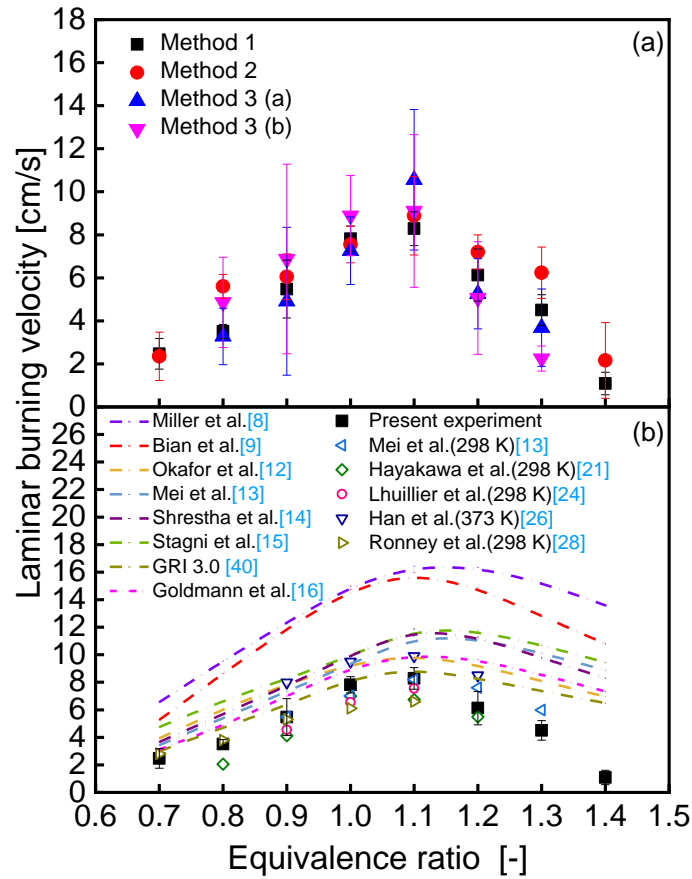
on the local place on the front surface of the flame. The error bars, i.e., the standard deviation, of the

344

data by the method 1 are relatively small compared to other methods. Therefore, it is used for

345

comparison and discussion in the following paragraphs.



346

347 **Fig. 8.** Laminar burning velocity of the ammonia/air mixtures under various equivalence ratios

348 ($P_0 = 0.1$ MPa and $T_0 = 360$ K). Symbols refer to the experimental results in this paper and in

349 previous studies [13, 21, 24, 26, 28]. Lines are the simulation results using different kinetic models

350 [8, 9, 12-15, 40] and calculation results by the correlations of Goldman et al. [16].

351 Fig. 8(b) includes the experimental results of the laminar burning velocities of this research, as

352 well as the experimental results of Hayakawa et al. [21], Mei et al. [13], Lhuillier et al. [24], Han et al.

353 [26] and Ronney et al. [28]. Plotted in Fig. 8(b) are also the simulation results using the reaction

354 mechanisms by Miller et al. [8], Bian et al. [9], Okafor et al. [12], Mei et al. [13], Shrestha et al. [14],

355 Stagni et al. [15] and the GRI 3.0 mechanism [40], respectively. The laminar burning velocity

356 correlations developed by Goldman et al. [16] is also included here based on the present experimental

357 conditions. As the equivalence ratio increases, all the laminar burning velocities obtained by either the

358 experiments or simulations increase at first, reach peaks around ϕ of 1.1, and then decrease. The
359 experimental peak laminar burning velocities are less than 9 cm/s and lower than most hydrocarbon
360 fuels. According to the Arrhenius dynamics, the laminar burning velocity is mainly affected by the
361 adiabatic flame temperature, and the trend of both of them versus equivalence ratio is almost identical
362 [50].

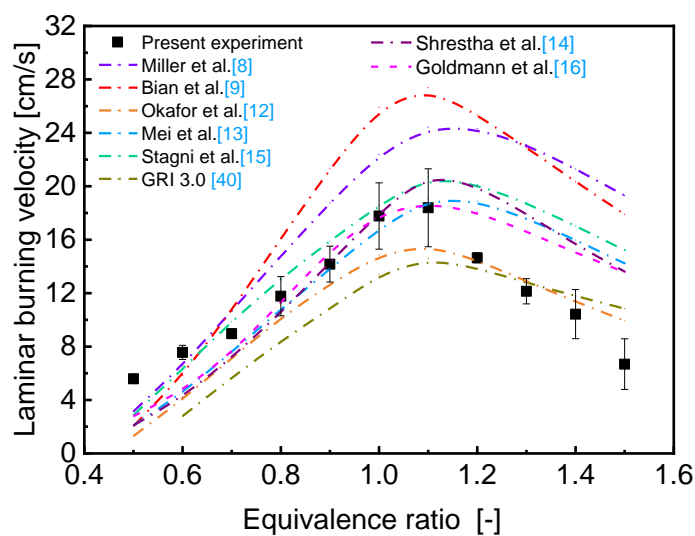
363 The simulations using different mechanisms lead to rather large variations at the fixed equivalence
364 ratio, though the general trend of the laminar burning velocity for various equivalence ratios is similar.
365 The kinetic models of Miller et al. [8] and Bian et al. [9] lead to great overpredictions for all the
366 equivalence ratios. The calculation using the GRI 3.0 mechanism shows the best agreement with the
367 experimental results among the existing mechanisms for the equivalence ratios below 1.1. For richer
368 mixtures, however, all the mechanisms as well as the correlations by Goldmann et al. [16] remarkably
369 overpredict the experimental results. Particularly, at the equivalence ratio of 1.4, the GRI 3.0
370 mechanism overpredicts by a factor of 6. Therefore, the chemical reaction mechanism of ammonia
371 combustion, especially at higher equivalence ratios than stoichiometric, needs to be further improved
372 based on the experimental data.

373 As the spherical flame spreads outwardly, the radiation effects should be taken into account
374 because it affected the laminar burning velocity. The flame temperature was influenced by the thermal
375 and flow effect induced by radiation and thus the spherical flame propagation speed was reduced by
376 the radiation cooling [49]. The following empirical correlation proposed by Yu et al. [49] can quantify
377 radiation-induced reduction in laminar burning velocity:

$$378 \quad RL = 0.82 \left(\frac{S_L}{S_i} \right)^{-1.14} \left(\frac{T_u}{T_i} \right) \left(\frac{P}{P_i} \right)^{-0.3} \quad (12)$$

379 where $S_i = 1$ cm/s, $T_i = 298$ K, and $P_i = 101325$ Pa. For the experimental peak laminar burning velocity
 380 in the present work, the radiation loss was 8.93%. Therefore, the laminar burning velocity under the
 381 adiabatic conditions can be obtained after compensating for the radiation loss and it was 9.02 cm/s that
 382 is 8.21% higher than the uncorrected value.

383 **Fig. 9** shows the results of the laminar burning velocity changing with the equivalence ratio for the
 384 fuel of 80% ammonia and 20% hydrogen. The initial ambient pressure is 0.1 MPa and the initial
 385 ambient temperature is 360 K. The error bar is relatively large for ϕ of 1.0 and 1.1, which may be
 386 related to the instability of the laminar flame when the laminar burning velocity is fast for the thermal
 387 expansion rate, σ , is relatively large. Plotted in **Fig. 9** are also for the simulation results using the
 388 reaction mechanisms. As the equivalence ratio increases, the laminar burning velocities of the
 389 ammonia/hydrogen/air mixtures show a similar trend with the ammonia/air mixtures. When the
 390 equivalence ratio is below 0.6, the simulations by all the kinetic models underpredict the experimental
 391 results, while most of these models lead to overpredictions for the equivalence ratio above 1.2. For the
 392 equivalence ratios from 0.7 to 1.1, the models by Mei et al. [13], Shrestha et al. [14] and Goldman's
 393 correlations [16] exhibit the better predictive performance than the others.



394

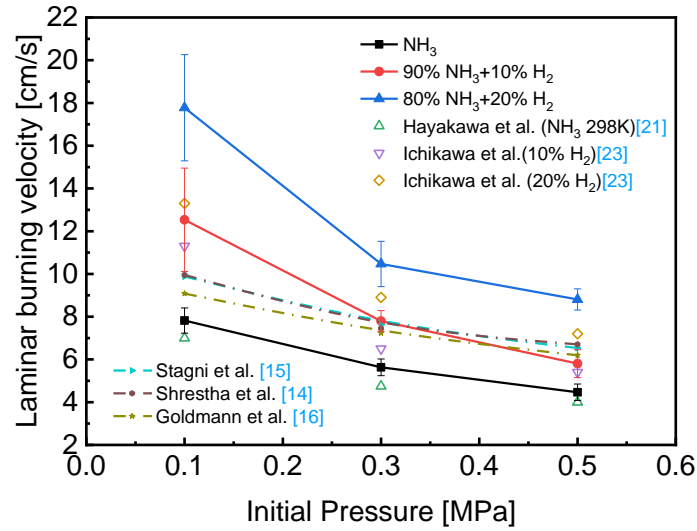
395 **Fig. 9.** Laminar burning velocity of the ammonia/hydrogen/air mixtures under various equivalence
396 ratios ($X_{H_2} = 20\%$, $P_0 = 0.1$ MPa and $T_0 = 360$ K). Symbols refer to the experimental results in this
397 study while lines are the simulation results using different kinetic models [8, 9, 12-15, 40] and the
398 calculation results by the correlations of Goldmann et al. [16].

399 3.3.2 Effects of initial ambient pressure

400 **Fig. 10** shows the laminar burning velocity under various initial ambient pressures with ϕ of 1.0
401 and T_0 of 360 K for the three fuels. Also shown are the results by Hayakawa [21] and Ichikawa et al.
402 [23] for comparison. The higher initial ambient temperature in the present experiments, i.e., 360 K,
403 than 298 K in Hayakawa's work, lead to the higher laminar burning velocity. As shown in **Fig. 10**, the
404 laminar burning velocity nonlinearly decreases with the initial ambient pressure increasing. According
405 to Law et al. [51], the relationship between the laminar burning velocity and the initial ambient
406 pressure is expressed by

$$407 \quad S_L \propto P_0^{\frac{n}{2}-1} \quad (13)$$

408 where n is the order of the total reaction. Since the oxidation reaction of ammonia and hydrogen is
409 mainly affected by the two-body branching and carrying reactions [8, 9, 12-15, 40], for example, $O +$
410 $H_2 = H + OH$, when the initial ambient pressure is low, n is close to 2 but less than 2 [50, 51]. With the
411 initial ambient pressure becoming higher, the increase in the three-body termination reactions, for
412 example, $O + H + M = OH + M$, will make n further reduced [51]. As a result, there is a negative
413 correlation between the laminar burning velocity and the initial ambient pressure.



414

415 **Fig. 10.** Laminar burning velocity of the ammonia/hydrogen/air mixtures under various initial

416 ambient pressures ($\phi = 1.0$ and $T_0 = 360$ K). Symbols refer to the experimental results

417 in this paper and in previous studies [21, 23] while lines are the simulation results using different

418 kinetic models [14, 15] and calculation results by the correlations of Goldmann et al. [16].

419 **Table 3** shows the coefficients of the pressure dependence extracted from the experimental or

420 numerical data in Fig. 10. The coefficient of the pressure dependence became smaller when the

421 hydrogen was added based on the present experimental results and such reduction can also be observed

422 from the data by Hayakawa et al. [21] and Ichikawa et al. [23]. In addition, the laminar burning velocity

423 changed more gently with the initial pressure from the simulation results using the mechanisms by

424 Shrestha et al. [14] and Stagni et al. [15]. Considering the experimental conditions of this paper into

425 the correlations in [16], a more gentle coefficient, -0.164, can be obtained. Therefore, the poor

426 performance on the prediction of the coefficient indicates that both the kinetic models and the

427 correlations should be improved.

428

Table 3. Coefficient of the pressure dependence

NH ₃ (present work)	-0.332
--------------------------------	--------

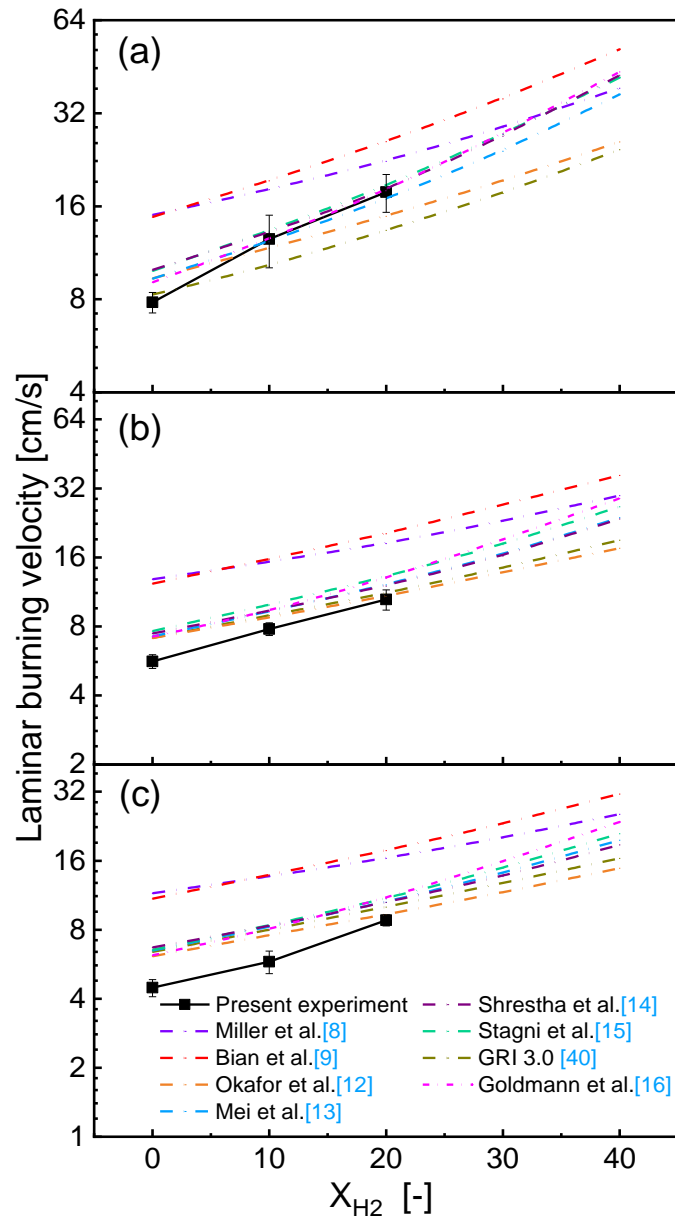
90% NH ₃ +10%H ₂ (present work)	-0.461
80% NH ₃ +20%H ₂ (present work)	-0.453
Hayakawa (NH ₃) [21]	-0.349
Ichikawa (10%H ₂) [23]	-0.475
Ichikawa (20%H ₂) [23]	-0.396
Shrestha et al. [14]	-0.251
Stagni et al. [15]	-0.251
Goldmann et al. [16]	-0.164

429 3.3.3 Effects of hydrogen contents

430 **Fig. 11** shows the experimental and simulation results of the laminar burning velocities varying
431 with the proportion of hydrogen contents under different initial ambient pressures. As shown in the
432 figures, under the three initial pressures, with the hydrogen contents increasing, the laminar burning
433 velocity increases. This confirms that the chemical reactivity of hydrogen is relatively high, and it can
434 significantly accelerate the combustion of ammonia. In the logarithmic graph, the laminar burning
435 velocity and the proportion of hydrogen contents show an approximately linear positive correlation.
436 When the proportion of hydrogen contents reaches 40%, the laminar burning velocity of the ammonia
437 mixtures is comparable to that of methane at the stoichiometric ratio, i.e. 30-40 cm/s.

438 Regarding the predictability of the existing kinetic models, as shown in **Fig. 11(a)**, the simulation
439 results using Mei et al. [13], Shrestha et al. [14], Stagni et al. [15] mechanism and Goldmann's
440 correlations [16] show the best predictive performance with the experimental values of the
441 ammonia/air mixtures and the ammonia/hydrogen/air mixtures at P_0 of 0.1 MPa, respectively.
442 However, as shown in **Fig. 11(b) & (c)**, with the initial ambient pressure becoming higher, the

443 simulation results obtained from the seven mechanisms as well as Goldmann's correlations [16] all
 444 overpredict the experimental values, indicating that the chemical reaction mechanism of the
 445 ammonia/hydrogen oxidation under the high pressures needs to be further revised.



446

447 **Fig. 11.** Laminar burning velocity of the ammonia/hydrogen/air mixtures under various proportions
 448 of hydrogen contents. The initial pressure of (a), (b) and (c) are 0.1 MPa, 0.3 MPa and 0.5 MPa,
 449 respectively, ($\phi = 1.0$ and $T_0 = 360$ K). Symbols refer to the experimental results in this study and

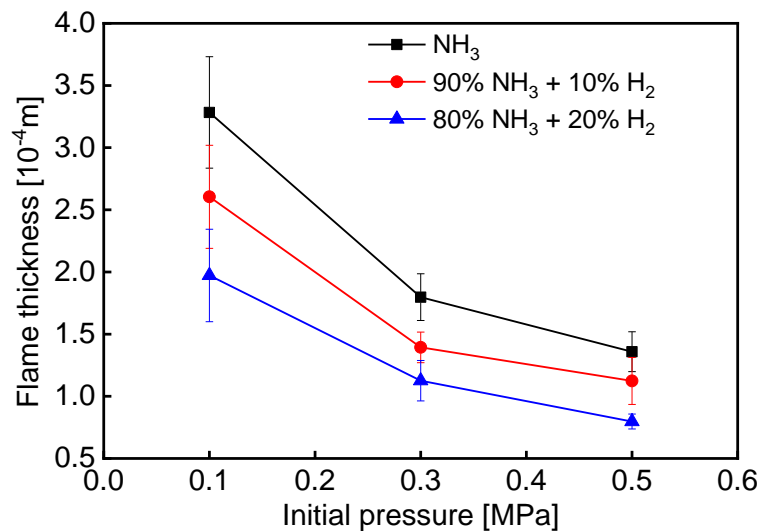
450 lines are the simulation results by different kinetic models [8, 9, 12-16, 40] and the calculation
451 results by the correlations of Goldmann et al. [16].

452

453 3.4 Flame thickness

454 Fig. 12 shows the results of the flame thickness under the various initial ambient pressures at ϕ of
455 1.0. The flame thickness here is calculated by Eq. (11), based on the experimental values of the laminar
456 burning velocity obtained in this work. As shown in Fig. 12, the flame thickness has a negative
457 correlation with the initial ambient pressure as well as the proportion of hydrogen contents. This is
458 also consistent with the previous analysis of flame instability in section 3.1. When the hydrogen
459 fraction and the initial ambient pressure are higher, the flame is more susceptible to the hydraulic
460 instability at the late stages of flame development, resulting in the cellular instability.

461



462

463 **Fig. 12.** Flame thickness of the ammonia/hydrogen/air mixtures under various initial ambient
464 pressures for the three fuels ($\phi = 1.0$ and $T_0 = 360$ K). Symbols refer to the experimental results in
465 this study.

466 4. Summary and conclusions

467 The laminar burning characteristics of the premixed ammonia/hydrogen/air mixtures have been
468 studied with the experiments and simulations. The effects of equivalence ratio (0.7-1.4), initial ambient
469 pressure (0.1MPa-0.5 MPa), hydrogen fraction (0-20%) on the laminar burning velocity are
470 investigated under the initial ambient temperature of 360K. The major conclusions are summarized as
471 follows:

- 472 • The ammonia/air mixtures can be ignited for an equivalence ratio range from 0.7 to 1.4 using
473 laser ignition, and the flame can spread stably.
- 474 • The laminar burning velocity of the ammonia/hydrogen/air mixtures increases firstly, reaches
475 the peak at the equivalence ratio around 1.1, and then decreases with the equivalence ratio
476 increasing from 0.7 to 1.4.
- 477 • The peak laminar burning velocities of the ammonia/air mixtures are lower than 9 cm/s, which
478 are significantly lower than those of hydrocarbon fuels.
- 479 • The simulations using different mechanisms lead to rather large variations at the fixed
480 equivalence ratio, though the general trend of the laminar burning velocity varied with the
481 equivalence ratio is similar. The numerical values of laminar burning velocities are mostly
482 above that of experiments for the ammonia/air mixtures. While the models except for those by
483 Miller and Bian can give reasonable predictions compared to the experimental results for the
484 equivalence ratio from 0.7 to 1.1 in the ammonia (80%)/hydrogen (20%)/air mixtures, all the
485 models overpredict the experiments for the richer mixtures. Therefore, the chemical reaction
486 mechanism of ammonia combustion, especially at the high equivalence ratios, needs to be

487 further improved. All the experimental results in this paper can be as the data reference for the
488 validation of kinetic models.

- 489 • As the initial ambient pressure increases, the laminar burning velocity of the
490 ammonia/hydrogen/air mixtures nonlinearly decreases, and the duration of heat releasing
491 becomes longer.
- 492 • The addition of hydrogen can significantly accelerate the laminar burning velocity of the
493 mixtures. The laminar burning velocity and the proportion of hydrogen contents show an
494 approximately linear positive correlation in the logarithmic graph, which provides a data
495 reference for the issue of enhancing the combustion intensity of ammonia.
- 496 • The cellular instability can be observed at the late stage of the ammonia/hydrogen/air flames
497 propagation when the proportion of hydrogen contents is 20% and the initial ambient pressure
498 is 0.5 MPa, which is related to the thin flame thickness due to the high hydrogen fraction and
499 the high initial ambient pressure.

500 **Acknowledgements**

501 The supports by the Major International (Regional) Joint Research Project of National Natural
502 Science Foundation of China (52020105009) and the National Natural Science Foundation of China
503 (51776125) are gratefully acknowledged. The assistances by Xinyi Zhou, Xinran Wang and other
504 students in the Large Engine Research Center of SJTU are highly appreciated.

505 **References**

- 506 [1] Schleussner C-F, Rogelj J, Schaeffer M, Lissner T, Licker R, Fischer EM, et al. Science and policy
507 characteristics of the Paris Agreement temperature goal. *Nat Clim Change* 2016;6(9):827-35.

- 508 [2] Giddey S, Badwal SPS, Munnings C, Dolan M. Ammonia as a Renewable Energy Transportation
509 Media. ACS Sustainable Chem Eng 2017;5:10231-39.
- 510 [3] Camilo Casallas, Ibrahim Dincer. Assessment of an integrated solar hydrogen system for
511 electrochemical synthesis of ammonia. Int J Hydrogen Energ 2017; 42(33): 21495-500.
- 512 [4] Armijo Julien, Philibert Cédric. Flexible production of green hydrogen and ammonia from variable
513 solar and wind energy: Case study of Chile and Argentina. Int J Hydrogen Energ 2020;45(3):1541-
514 58.
- 515 [5] Wang L, Xia M, Wang H, Huang K, Qian C, Maravelias CT, et al. Greening Ammonia toward the
516 Solar Ammonia Refinery. Joule 2018;2(6):1055-74.
- 517 [6] Valera-Medina A, Xiao H, Owen-Jones M, David WIF, Bowen PJ. Ammonia for power. Prog
518 Energy Combust Sci 2018;69:63-102.
- 519 [7] Kobayashi H, Hayakawa A, Somarathne KDKA, Okafor EC. Science and technology of ammonia
520 combustion. Proc Combust Inst 2019;37(1):109-33.
- 521 [8] Miller JA, Smooke MD, Green RM, Kee RJ. Kinetic Modeling of the Oxidation of Ammonia in
522 Flames. Combust Sci Technol 1983;34(1-6):149-76.
- 523 [9] Bian J, Vandooren J, Van Tiggelen PJ. Experimental study of the formation of nitrous and nitric
524 oxides in H₂-O₂-Ar flames seeded with NO and/or NH₃. Symp (Int) Combust 1991;23(1):379-
525 86.
- 526 [10] Lindstedt RP, Lockwood FC, Selim MA. A Detailed Kinetic Study of Ammonia Oxidation.
527 Combust Sci Technol 1995;108(4-6):231-54.
- 528 [11] Tian Z, Li Y, Zhang L, Glarborg P, Qi F. An experimental and kinetic modeling study of premixed
529 NH₃/CH₄/O₂/Ar flames at low pressure. Combust Flame 2009;156(7):1413-26.

- 530 [12]Okafor EC, Naito Y, Colson S, Ichikawa A, Kudo T, Hayakawa A, et al. Measurement and
531 modelling of the laminar burning velocity of methane-ammonia-air flames at high pressures using
532 a reduced reaction mechanism. *Combust Flame* 2019;204:162-75.
- 533 [13]Mei B, Zhang X, Ma S, Cui M, Guo H, Cao Z, et al. Experimental and kinetic modeling
534 investigation on the laminar flame propagation of ammonia under oxygen enrichment and elevated
535 pressure conditions. *Combust Flame* 2019;210:236-46.
- 536 [14]Shrestha KP, Lhuillier C, Barbosa AA, Brequigny P, Contino F, Mounaïm-Rousselle C, et al. An
537 experimental and modeling study of ammonia with enriched oxygen content and
538 ammonia/hydrogen laminar flame speed at elevated pressure and temperature. *Proc Combust Inst*
539 2020;000:1-12.
- 540 [15]Stagni A, Cavallotti C, Arunthanayothin S, Song Y, Herbinet O, Battin-Leclerc F, Faravelli T. An
541 experimental, theoretical and kinetic-modeling study of the gas-phase oxidation of ammonia. *React*
542 *Chem Eng* 2020;5:697-771.
- 543 [16]Goldmann A, Dinkelacker F. Approximation of laminar flame characteristics on premixed
544 ammonia/hydrogen/nitrogen/air mixtures at elevated temperatures and pressures. *Fuel*
545 2018;224:366-378.
- 546 [17]Mathieu O, Petersen EL. Experimental and modeling study on the high-temperature oxidation of
547 ammonia and related NO_x chemistry. *Combust Flame* 2015;162(3):554–70.
- 548 [18]Hu E, Huang Z, Liu B, Zheng J, Gu X, Huang B. Experimental investigation on performance and
549 emissions of a spark-ignition engine fuelled with natural gas–hydrogen blends combined with
550 EGR. *Int J Hydrogen Energ* 2009;34(1):528-39.

- 551 [19]Pfahl UJ, Ross MC, Shepherd JE, Pasamehmetoglu KO, Unal C. Flammability Limits, Ignition
552 Energy, and Flame Speeds in H₂–CH₄–NH₃–N₂O–O₂–N₂ Mixtures. *Combust Flame*
553 2000;123(1-2):140–58.
- 554 [20]Takizawa K, Takahashi A, Tokuhashi K, Kondo S, Sekiya A. Burning velocity measurements of
555 nitrogen-containing compounds. *J Hazard Mater* 2008;155(1-2):144-52.
- 556 [21]Hayakawa A, Goto T, Mimoto R, Arakawa Y, Kudo T, Kobayashi H. Laminar burning velocity
557 and Markstein length of ammonia/air premixed flames at various pressures. *Fuel* 2015;159:98-106.
- 558 [22]Xiao P, Wu H, Wang Z, Zhang S, Lee Chia-fon, Wang Z, et al. Experimental and kinetic
559 investigation on the effects of hydrogen additive on laminar premixed methanol–air flames. *Int J*
560 *Hydrogen Energ* 2019;44:22263-81.
- 561 [23]Ichikawa A, Hayakawa A, Kitagawa Y, Kunkuma Amila Somarathne K D, Kudo T, Kobayashi
562 H. Laminar burning velocity and Markstein length of ammonia/hydrogen/air premixed flames at
563 elevated pressures. *Int J Hydrogen Energ* 2015;40(30):9570-78.
- 564 [24]Lhuillier C, Brequigny P, Lamoureux N, Contino F, Mounaïm-Rousselle C. Experimental
565 investigation on laminar burning velocities of ammonia/hydrogen/air mixtures at elevated
566 temperatures. *Fuel* 2020;263:116653.
- 567 [25]Davis SG, Pagliaro JL, Debold TF, Wingerden M, Wingerden K. Flammability and explosion
568 characteristics of mildly flammable refrigerants. *J Loss Prevent Proc* 2017;49:662-74.
- 569 [26]Han X, Wang ZH, He Y, Liu Y, Zhu Y, Konnov AA. Experimental investigation on laminar
570 burning velocities of ammonia/hydrogen/air mixtures at elevated temperatures. *Combust Flame*
571 2020;217:314–20.

- 572 [27]Zakaznov VF, Kursheva LA, Fedina ZI. Determination of normal flame velocity and critical
573 diameter of flame extinction in ammonia-air mixture. *Combust Explos Shock Waves* 1978;14:
574 710–13.
- 575 [28]Ronney PD. Effect of Chemistry and Transport Properties on Near-Limit Flames at Microgravity.
576 *Combust Sci Technol* 1988;59(1-3):123-41.
- 577 [29]Dhananjay Kumar Srivastva, Avinash Kumar Agarwal. Laser Ignition of Hydrogen-Air Mixture
578 in a Combustion Bomb. SAE paper 2008-28-0033; 2008.
- 579 [30]Xu C, Fang D, Luo Q, Ma J, Xie Y. A comparative study of laser ignition and spark ignition with
580 gasoline–air mixtures. *Opt Laser Technol* 2014;64:343-51.
- 581 [31]Pal Anuj, KA Avinash. Comparative study of laser ignition and conventional electrical spark
582 ignition systems in a hydrogen fuelled engine. *Int J Hydrogen Energy* 2015;40(5):2386-95.
- 583 [32]Liedel G, Schuocker D, Geringer B, Graf J, Klawatsch D, Lenz HP, et al. Laser induced ignition
584 of gasoline direct injection engines. *Proceeding SPIE* 2005;5777:955-60.
- 585 [33]NIST, NIST Chemistry WebBook: NIST Standard Reference Database Number 69. <
586 <http://webbook.nist.gov/chemistry/>>.
- 587 [34]Bradley D, Gaskell PH, Gu XJ. Burning velocities, Markstein lengths, and flame quenching for
588 spherical methane-air flames: A computational study. *Combust Flame* 1996;104:176-98.
- 589 [35]Bradley D, Hicks RA, Lawes M, Sheppard CGW, Woolley R. The measurement of laminar
590 burning velocities and Markstein numbers for iso-octane-air and iso-octane-n-heptane-air mixtures
591 at elevated temperatures and pressures in an explosion bomb. *Combust Flame* 1998;115:126-44.
- 592 [36]Burke MP, Chen Z, Ju Y, Dryer FL. Effect of cylindrical confinement on the determination of
593 laminar flame speeds using outwardly propagating flames. *Combust Flame* 2009;156(4):771-79.

- 594 [37]P Clavin. Dynamic behaviour of premixed flame fronts in laminar and turbulent flows, Prog
595 Energy Combust Sci 1985;11:1–59.
- 596 [38]Hu E, Huang Z, He J, Zheng J, Miao H. Experimental and numerical study on laminar burning
597 velocities and flame instabilities of hydrogen–air mixtures at elevated pressures and temperatures.
598 Int J Hydrogen Energy 2009;34:8741-55.
- 599 [39]Wu F, Liang W, Chen Z, Ju Y, Law CK. Uncertainty in stretch extrapolation of laminar flame
600 speed from expanding spherical flames, Proc Combust Inst 2015;35:663-70.
- 601 [40]Frenklach M, Bowman T, Smith G. GRI-Mech 3.0. 2000. <[http://www.me.berkeley.edu/gri-](http://www.me.berkeley.edu/gri-mech/index.html)
602 [mech/index.html](http://www.me.berkeley.edu/gri-mech/index.html)>.
- 603 [41]Bechtold JK, Matalon M. The dependence of the Markstein length on stoichiometry. Combust
604 Flame 2001;127:1906-1913.
- 605 [42]de Goey LPH, Hermanns RTE, Bastiaans RJM. Analysis of the asymptotic structure of
606 stoichiometric premixed CH₄–H₂–air flames. Proc Combust Inst 2007; 31:1031-1038.
- 607 [43]Dinkelacker F, Manickam B, Muppala SPR. Modelling and simulation of lean premixed turbulent
608 methane/hydrogen/air flames with an effective Lewis number approach. Combust Flame 2011;
609 158:1742-49.
- 610 [44]Law CK, Jomaas G, Bechtold JK. Cellular instabilities of expanding hydrogen/propane spherical
611 flames at elevated pressures: theory and experiment. Proc Combust Inst 2005;30(1):159-67.
- 612 [45]Bechtold JK, Matalon M. Hydrodynamic and diffusion effects on the stability of spherically
613 expanding flames. Combust Flame 1987;67(1):77-90.
- 614 [46]Parlange JY. Influence of Preferential Diffusion on the Stability of a Laminar Flame. J Chem Phys
615 1968;48(4):1843-49.

- 616 [47]Matalon M, Cui C, Bechtold JK. Hydrodynamic theory of premixed flames: effects of
617 stoichiometry, variable transport coefficients and arbitrary reaction orders. J Fluid Mech
618 2003;487:179-210.
- 619 [48]Hu E, Huang Z, He J, Zheng J, Miao H. Measurements of laminar burning velocities and onset of
620 cellular instabilities of methane–hydrogen–air flames at elevated pressures and temperatures. Int J
621 Hydrogen Energy 2009;34(13):5574-84.
- 622 [49]Yu H, Han W, Santner J, Gou X, Sohn CH, Ju Y, et al. Radiation-induced uncertainty in laminar
623 flame speed measured from propagating spherical flames. Combust Flame 2014. 161: 2815-24.
- 624 [50]Law CK. Combustion physics. Cambridge University Press; 2006, p. 275-82.
- 625 [51]Egolfopoulos F, Law CK. Chain mechanisms in the overall reaction orders in laminar flame
626 propagation. Combust Flame 1990;80(1):7-16.

627 **Nomenclature**

- 628 A_f projection area of the burned zone [mm^2]
- 629 C_p specific heat at constant pressure [W/kg/K]
- 630 E_a activation energy [J]
- 631 H_2 hydrogen
- 632 H_2O water
- 633 L_b Markstein length [cm]
- 634 Le Lewis number [-]
- 635 Le_D Lewis number of the deficient reactant [-]
- 636 Le_E Lewis number of the excess reactant [-]

637	Le_{eff}	effective Lewis number [-]
638	Le_i	Lewis number of species i [-]
639	n	order of the total reaction [-]
640	N_2	nitrogen
641	N_2O	nitrous Oxide
642	NH_3	ammonia
643	NO	nitric oxide
644	O_2	oxygen
645	CVCC	constant volume combustion chamber
646	p	real-time ambient pressure in the CVCC [MPa]
647	P_0	initial ambient pressure [MPa]
648	Q	apparent heat released during the combustion [J]
649	S_L	laminar burning velocity [cm/s]
650	R	gas constant [-]
651	RL	Radiative loss [%]
652	r_f	equivalent radius of the flame [mm]
653	S_b^0	unstretched speed [cm/s]
654	S_b	stretched speed [cm/s]
655	T_{ad}	adiabatic flame temperature [K]
656	T_0	initial ambient temperature [K]
657	T_{inner}	inner layer temperature [K]
658	V_{CVCC}	volume of the CVCC [L]

659	V_{H_2}	volume of hydrogen in the mixed fuel [m ³]
660	X_{H_2}	volumetric percentage of hydrogen in the mixed fuel [%]
661	X_{NH_3}	volumetric percentage of ammonia in the mixed fuel [%]
662	Δy	distance between the top and bottom of the flame kernel [mm]
663	Ze	Zel'dovich number [-]
664	α	thermal diffusivity [10 ⁻⁵ m ² /s]
665	δ	flame thickness [10 ⁻⁴ m]
666	ε	stretch rate of the flame [1/s]
667	ϕ	equivalence ratio [-]
668	κ	isentropic index [-]
669	λ	thermal conductivity [10 ⁻² W/m/K]
670	ρ_b	density of burned gas [kg/m ³]
671	ν	kinematic viscosity [10 ⁻⁵ m ² /s]
672	ρ_u	density of unburned gas [kg/m ³]
673	σ	thermal expansion rate [-]